frontiers in Mechanical Engineering

ORIGINAL RESEARCH
published: 27 June 2016
doi: 10.3389/fmech.2016.00005

Design and Microfabrication Considerations for Reliable Flexible Intracortical Implants

Harbaljit S. Sohal[1,2], Konstantin Vassilevski[3], Andrew Jackson[4], Stuart N. Baker[4] and Anthony O'Neill[3]*

[1] Media Lab, McGovern Institute, MIT, Cambridge, MA, USA, [2] Microsystems Technology Laboratories, MIT, Cambridge, MA, USA, [3] School of Electrical and Electronic Engineering, Newcastle University, Newcastle upon Tyne, UK, [4] Institute of Neuroscience, Newcastle University, Newcastle upon Tyne, UK

Current microelectrodes designed to record chronic neural activity suffer from recording instabilities due to the modulus mismatch between the electrode materials and the brain. We sought to address this by microfabricating a novel flexible neural probe. Our probe was fabricated from parylene-C with a tungsten–titanium alloy metal, using contact photolithography and reactive-ion etching, with three design features to address this modulus mismatch: a sinusoidal shaft, a rounded tip, and a polyimide anchoring ball. The anchor restricts movement of the electrode-recording sites, and the shaft accommodates the brain motion. We successfully patterned thick metal and parylene-C layers, with a reliable device release process leading to high functional yield. This novel, reliably microfabricated, probe can record stable neural activity for up to 2 years without delamination, surpassing the current state-of-the-art intracortical probes. This challenges recent concerns that have been raised over the long-term reliability of chronic implants when parylene-C is used as an insulator, for both research and human applications. The microfabrication and design considerations provided in this manuscript may aid in the future development of flexible devices for biomedical applications.

Keywords: flexible, parylene, tungsten, brain, micromotions

OPEN ACCESS

Edited by:
Andreas Dietzel, Technische Universität Braunschweig, Germany

Reviewed by:
Qin Zhou, University of California, Berkeley, USA
Theodor Doll, Hannover Medical School, Germany

****Correspondence:***
Harbaljit S. Sohal
hssohal@mit.edu

Specialty section:
This article was submitted to Micro- and Nanoelectromechanical Systems, a section of the journal Frontiers in Mechanical Engineering

Received: *30 April 2016*
Accepted: *13 June 2016*
Published: *27 June 2016*

Citation:
Sohal HS, Vassilevski K, Jackson A, Baker SN and O'Neill A (2016) Design and Microfabrication Considerations for Reliable Flexible Intracortical Implants. Front. Mech. Eng. 2:5. doi: 10.3389/fmech.2016.00005

INTRODUCTION

Chronically implanted intracortical microelectrodes have been used in invasive brain machine interfaces (BMI) for controlling computers and assistive devices to restore function after paralysis (Hochberg et al., 2006, 2012; Collinger et al., 2013). However, current devices suffer from recording instabilities that lead to loss of cells over time (Dickey et al., 2009). One reason for this is the Young's modulus mismatch between electrode materials and brain tissue, leading to micromotion-induced trauma (Subbaroyan et al., 2005; Dickey et al., 2009) and a persistent immune response that compromises neural function (Polikov et al., 2005).

One way to mitigate the Young's modulus (E) mismatch is to produce flexible interfaces for long-term implants (Gilletti and Muthuswamy, 2006). Current flexible electrodes are centered on the use of polymers, such as parylene-C ($E = 2.86$ GPa), polyimide ($E \sim 2.3$ GPa), SU-8 ($E = 4.02$ GPa), and smart materials with a suitable metal for recording, although chronic recording data are lacking. Most of the current flexible devices seem to develop issues, especially for interfacing >1 year. For example, polyimide has been used extensively for flexible electrodes (Rubehn et al., 2009); however, it suffers from pinhole development, which will lead to subsequent *in vivo* device delamination

through fluid infiltration and is also ~3 times stiffer (in the case of PI-2611) than parylene-C-based electrodes (Rubehn and Stieglitz, 2007). Additionally, performing leak impedance measurements after submerging PI-2611 in 40°C saline found sharp declines in impedances after 2–3 days, alluding to insulation failure on probes, which would translate to poor *in vivo* performance. However, enhanced performance can be obtained, if specific curing measures are used (Ceyssens and Puers, 2015). Smart materials (Harris et al., 2011b; Hess et al., 2011; Ware et al., 2012) that change E when being inserted due to water uptake or a change in temperature (e.g., 5 GPa 12 MPa would be an ideal solution) suffer from poor insulating properties and have only been used as insertion aids for flexible structures or lack major characterization beyond a proof-of-principle demonstration (Ware et al., 2012). Furthermore, chronic implantation after 8 weeks showed a similar distribution of defect nuclei compared with a microwire electrode, therefore conferring no advantage to prolong chronic recording through modulus matching with these materials (Harris et al., 2011a,b). Conductive polymers (Lu et al., 2014) and carbon fibers have also been used; however, these lack *in vivo* characterization for indwelling periods >1 year (Yoshida Kozai et al., 2012) and seem to confer no advantage over conventional electrodes in terms of gliosis (Canales et al., 2015). Finally, carbon fiber probes, which can be produced at small diameters with $E = 241$ GPa (Patel et al., 2015), can be more stiff than inflexible silicon probes, although good chronic recording has still been obtained with such probes (Guitchounts et al., 2013).

In a previous study, we were able to record neural activity for >2-year periods, demonstrating the long-term reliability of our microfabricated devices (Sohal et al., 2014). The probe comprised a parylene-C–metal-parylene-C sandwich with design features to minimize the effects of micromotion. This study had an emphasis on the biological impact of such probes to address micromotion-induced trauma, such as high fidelity recording quality for up to 2 years and reduced foreign body response determined through histology, after chronic implantation.

Here, we report the refined design and microfabrication considerations that allowed reliable flexible devices to survive the challenging environment of chronic neural recording (Barrese et al., 2013). A novel use of the probe for acute electrophysiology is also presented. The overall details in this study will aid other groups involved in flexible microfabrication in potentially obtaining reliable devices for chronic interfacing, in a wide variety of biomedical applications.

DESIGN

Compared with the conventional rigid and sharp electrodes, the design had several features to minimize micromotion-induced trauma (**Figure 1A**). The probe was made out of flexible materials and incorporated a rounded tip with three protruding recording sites, which were anchored within the brain tissue with a polyimide ball. Further, the design incorporated a sinusoidal shaft, instead of a straight shaft. This shaft accommodates movement of the brain, mechanically decoupling the recording end from the surface fixation point and thus allowing the electrode sites and ball anchor to move freely with the tissue. The recording end of the probe was a parylene-C disk of 100 μm diameter, with three protruding, exposed recording sites (96 μm^2) to aid single-unit isolation. Three metal tracks (5 μm width and gap) ran within an electrode shaft that was 20 μm deep, 35 μm wide, and had a sinusoidal profile with cycles of 100 μm amplitude and 500 μm period. The probe was 3 mm in length and incorporated an integrated parylene-C-based ribbon cable (3 cm long and 3 mm wide) leading to a standard connector (micro ps1/ps2 series, Omnetics Connector Corporation, USA) (**Figures 1B,C**). To demonstrate the utility of a sinusoidal shaft, a finite element model (FEM) was constructed (**Figure 2**). GDS files from mask designs were imported into COMSOL Multiphysics®, for both straight and sinusoidal shafts with identical dimensions (3 mm length, 20 μm thick, and 35 μm wide) to form a 3D model. The "Solid Mechanics" physics was used, and the top of the electrode shaft was rigid ("fixed constraint"). Parylene-C was used in this simulation with properties of $E = 2.86$ GPa, density $= 1.29$ kg/m^3, and Poisson's ratio $= 0.4$. The shaft itself was free to move. We compared the flexibility of both designs to accommodate displacements in three dimensions. An arbitrary displacement (100 μm) was applied in the orthogonal X, Y, and Z directions of the rounded recording end for both the straight and sinusoidal probe design. **Figure 2** shows that a sinusoidal shaft, rather than a straight shaft, will deform more to counter movement of the probe primarily in the Y direction [Average displacement of the probes (±SEM) 85 ± 9 vs. 53 ± 9 μm^3, t-test: $t = 5.5$, $P < 0.001$] as calculated through COMSOL Multiphysics® using the "domain probe" feature, which allows the measurement of displacement values for the duration of the simulation. Comparable average displacement values (53.3 μm) were obtained for X and Z directions. The Y-direction has also been shown to be the primary axis of motion (cephalocaudal) for the brain in both rodents and human MR studies (Poncelet et al., 1992; Chen et al., 2010; Köhler et al., 2015).

The simulation allowed the assessment of the Von Mises stress on both the shank types. The von Mises stress is used to predict the yielding of materials under any loading condition from results of simple uniaxial tensile tests. The stress induced by the movement was significantly reduced for a sinusoidal (30.7 MPa) rather than a straight shaft (92.5 MPa), showing that it is also better at minimizing stresses on the shank and at accommodating random brain motion.

FABRICATION

Overall Process Flow

Fabrication began with deposition of 1-μm thick Al on a silicon carrier wafer by e-beam evaporation. Sequentially, the first parylene-C, tungsten–titanium alloy (WTi) metal, and final parylene-C layer were deposited through chemical vapor deposition and sputtering, respectively (**Figure 3A**) and patterned to form the conductive tracks and to define the overall shape of the sinusoidal probe (**Figure 3B**). WTi patterning occurred through SF_6 RIE, and parylene-C patterning occurred through RIE oxygen plasma. Devices were released through aluminum sacrificial layer etching with dilute TMAH (**Figure 3C**).

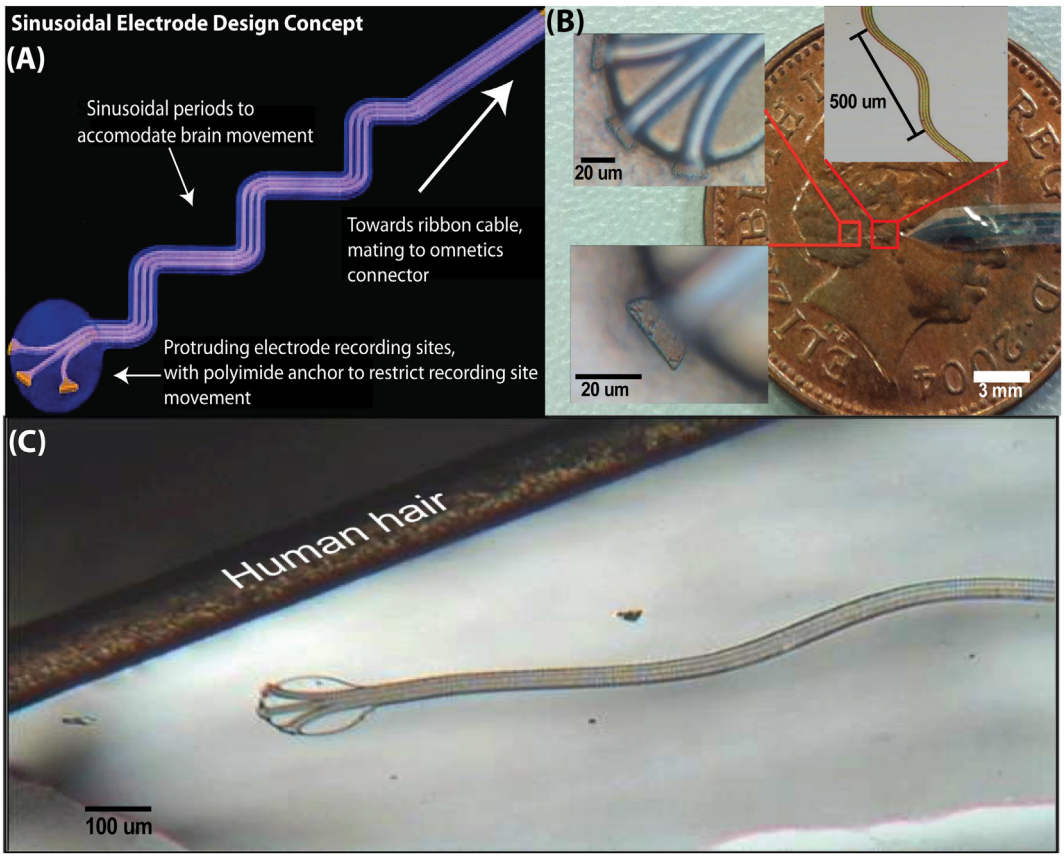

FIGURE 1 | The sinusoidal probe had design measures to reduce micromotion, such as anchored recording sites and a sinusoidal shaft to accommodate brain motion (A). Microfabricated probe compared with a one-penny coin with insets showing recording sites and sinusoidal shaft, respectively **(B)**. As a size comparison, the probe is shown against a human hair **(C)**.

Metalization

Tungsten–titanium alloy was used as the metal layer. Tungsten and has been used extensively for the past 50 years to record from the brain (Hubel, 1959) but is relatively stiff compared with other metals and was sintered with titanium using a combined metal sputtering target for increased flexibility (Young's modulus: 110 GPa).

To form conductive tracks in the electrodes, a 1-μm thick WTi layer was deposited by magnetron sputtering in a Kurt Lesker PVD 75 vacuum deposition system using a sintered target with WTi (80/20 wt%) from Pi-Kem Ltd. An unconventional 1-μm thick WTi metal was used for the tip-based recording sites, where the thickness of the metal defines the recording site area. The electrode-recording sites are four exposed faces of a cuboid. Overall, a 1-μm thick layer will yield a recording area of around 96 μm^2. Thinning the metal down to 500 nm will give a site area of 80 μm^2. A thicker metal would also be more resistant to potential chronic degradation of the metal due to electrochemistry, a further design measure used to enhance probe longevity (Williams et al., 2003).

RIE in SF_6 plasma (**Figure 4**) was chosen instead of a wet etch, as it provided a means to surface roughen the first parylene-C layer (improving overall parylene-C adhesion) by employing a simple "over-etch." Also, the RIE process has the advantage that it reduces the risk of parylene-C swelling during wet etching (Tooker et al., 2012). A novel wet etch was also performed with a mixture of ammonia hydroxide (30%) and hydrogen peroxide (30%) (1:1 ratio), and it was found that 1-μm thick WTi (80/20 wt%) was etched in 5 min. A 3-μm thick TI-35ES photoresist (HD Microchemicals, Germany) was used as a mask for this process.

Thick Parylene-C Etching

The chosen dielectric was parylene-C, due to excellent mechanical and electrical properties, including a low modulus of elasticity (2.86 GPa) and elongation at break of 200%, suitable to accommodate large deflections. Moreover, parylene-C has a high long-term dielectric constant due to a very low water uptake at 50% humidity (Loeb et al., 1977; Seymour and Kipke, 2007; Seymour et al., 2011). In addition to published literature, the film quality was observed between polyimide and parylene-C post-deposition. PI-5878G (HD MicroSystems, USA) was chosen to be a comparison dielectric to parylene-C due to similar electrical and mechanical properties. The polyimide

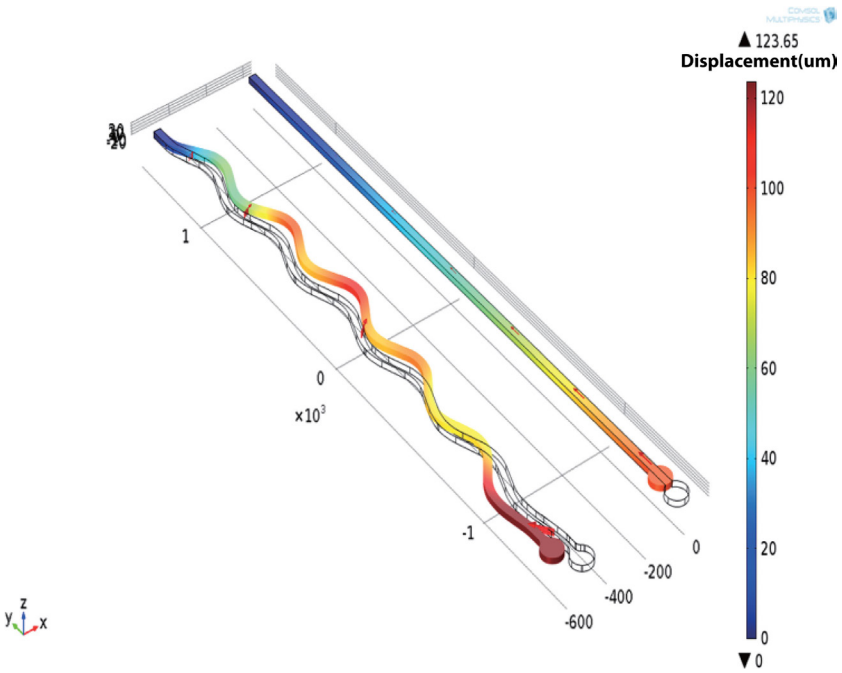

FIGURE 2 | COMSOL FEM showing the utility of a sinusoidal vs. a straight shaft. The sinusoidal shaft will deform more in the *Y*-direction, which is thought to be the primary axis of motion in the brain.

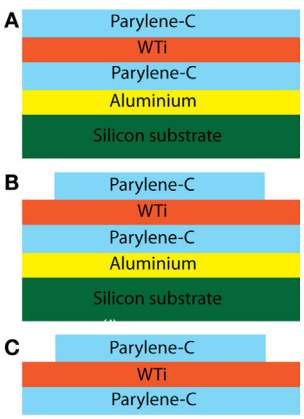

FIGURE 3 | Optimized process flow for the Sinusoidal probe. Al was deposited on a 3′′ wafer to aid the device release. Sequentially, the first parylene-C, WTi metal, and final parylene-C layer **(A)** were deposited and patterned **(B)** to form the conductive tracks and to define the overall shape of the sinusoidal probe. Finally, the device was released by etching the Al in weak TMAH [3%; **(C)**].

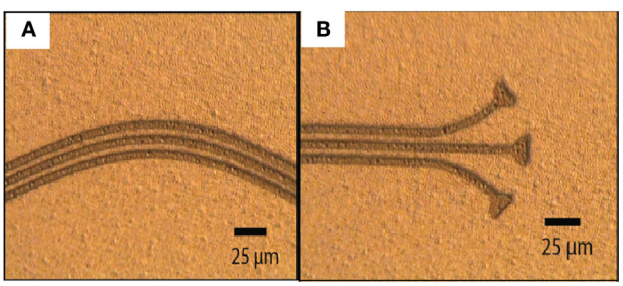

FIGURE 4 | Successfully patterned WTi metal with SF_6 RIE. There was limited dimension loss. RIE was preferred over the wet etch due to the ability to surface roughen the first parylene-C layer to aid parylene-C to parylene-C adhesion. The two optical images show various parts of the electrode design and successful patterning of unconventional features: sinusoidal electrode tracks **(A)** and recording sites **(B)**.

was deposited on to silicon wafers in accordance to manufacturer guidelines and cured N_2 environment at 350°C for 2 h to drive away any remaining solvent and for complete imidization.

Dielectric failure has been attributed to the accumulation of bubbles within the layer (Rubehn and Stieglitz, 2007), leading to pitting over time. A bubble test was performed on polyimide and parylene-C coated on 3′′ wafers with an aluminum sacrificial layer. Ten random images were taken for layers on ×5 optical magnifications. The number of bubbles per image was counted manually with the use of ImageJ64 software (NIH, USA). A *t*-test was then performed to compare the two groups. The polyimide layer had a significantly greater number ($t = 6.2$, $P < 0.001$) of bubbles than a parylene-C layer. An overall ratio for the number of bubbles in polyimide compared with parylene-C was calculated at 8:1. This reaffirmed the choice for parylene-C as the dielectric for our probe (**Figure 5**).

Relatively thick parylene-C films (20 µm) were etched using RIE in oxygen plasma. This thickness was chosen as a balance

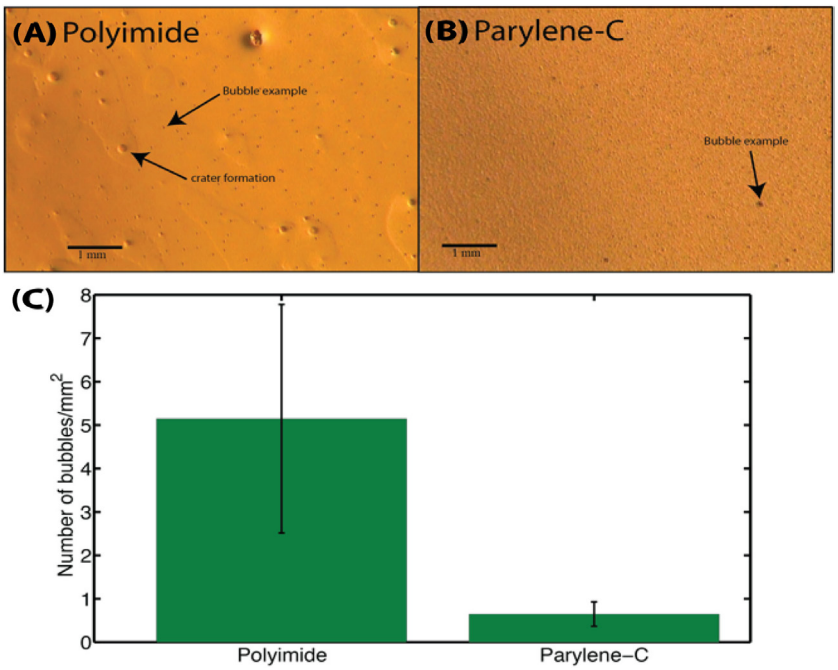

FIGURE 5 | Representative image of a polyimide (A) and parylene-C (B) layer. The parylene-C layer had a slightly rough aluminum layer underneath, and roughness is visible due to the conformal coating nature for parylene-C; bubble visualization remains unaffected. **(C)** Bubble comparison test for a polyimide and parylene-C layer. Overall, an 8:1 ratio is obtained for polyimide to parylene-C bubbles. For polyimide and parylene-C, mean ± SEM values of 5.15 ± 2.63 and 0.65 ± 0.28 bubbles/mm^2 are obtained, respectively. The greater variation for polyimide further adds unpredictability about dielectric performance in respect to potential pitting.

between flexibility and improved chronic performance vs. potential insulation degradation. Ti (40 nm thick) was used as a mask and patterned using diluted HF (HF:H_2O = 1:60) for 15 s (**Figure 6B**). An Al mask was found to be unsuitable for this process due to poor parylene-C adhesion (**Figure 6A**).

The parylene-C was subjected to RIE in oxygen plasma at room temperature, having a discharge power of 200 W, pressure of 50 mTorr, and gas flow rate of 18 sccm, this was found to be the optimum parameters. The RIE process provided an anisotropic etch of parylene-C with an etch rate of 230 nm/min and good selectivity to the exposed WTi and Al. Resultant sidewalls of fabricated electrodes were vertical as shown by optical (**Figure 6C**) and scanning electron microscopy (**Figure 6D**). To determine the side wall angles and etch isotropy, samples were appropriately cleaved to check the sidewall profile with the use of optical microscopy. Images were captured and the sidewall angles were measured from the optical images in the Matlab environment, as indicated by the red-dashed line in **Figure 5C** (2009a, MathWorks, USA). Parameters of 200 W and 50 mTorr pressure yielded vertical etch and had an angle of 88° ± 0.4° (n = 5 samples). Further, the vertical sidewalls were reconfirmed with scanning electron microscopy (**Figure 6D**). Parameters of 175 W and 100 mTorr pressure yielded less of a vertical etch and had an angle of 82° ± 0.6° (n = 7 samples). The Ti mask had minimal etching, with the Ti thickness still measuring 30–35 nm, after the etch.

Sacrificial Layer Choice and Device Release

Two sacrificial layer options were explored, with the use of PVD deposited SiO_2 and aluminum. SiO_2 etching with HF (49%) was often successful; however, the release process took >24 h, which risked damaging our completed probe (Seymour et al., 2011; Tooker et al., 2012).

Therefore, we used aluminum as a sacrificial layer. Depending on the adhesion, we released devices with either IPA, which allowed device release directly from the aluminum or etching the aluminum with dilute TMAH (e.g., AZ-326 MIF, photoresist developer, HD Microchemicals), the latter resulting in higher device yields. All devices were released within a 1.5-h period without underlying damage to the parylene-C or WTi.

DEVICE PACKAGING

Connector Attachment

Silver paint bonding was used to attach the connector to the probe. Gold wire wedge bonding and soldering were ruled out due to issues in obtaining reliable connections. Two layers of epoxy were sufficient to insulate the connector bond through leak impedance (1 kHz) measurements in saline, and epoxy had the advantage over polyimide insulation as it could be removed with *N*-Methyl-2-pyrrolidone (NMP) allowing connectors to be re-used.

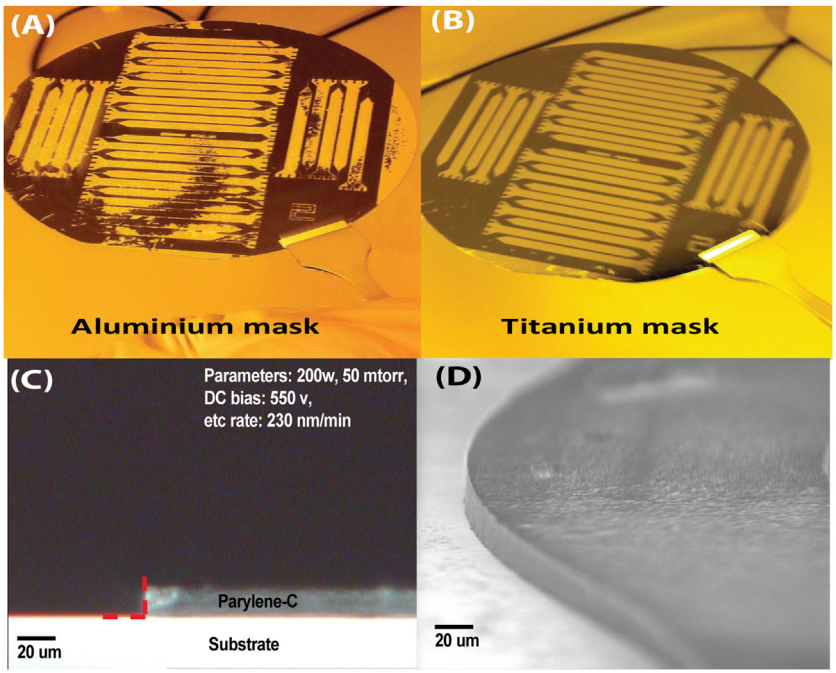

FIGURE 6 | Optimization of the thick layer parylene-C etching. A Ti hard mask **(B)** was preferred over Al **(A)** due to poor adhesion. Highly vertical side walls were achieved as corroborated through optical **(C)** and scanning electron microscopy (SEM). SEM picture is of the rounded recording end for the sinusoidal probe **(D)**.

Device Attachment to Insertion Carrier

In order to be implanted into the brain, the flexible electrode was attached temporarily to a rigid carrier using poly-ethylene-glycol (PEG: MW 6000) (Baker et al., 2008). After insertion, this was washed away with warm saline to liberate the electrode and allow removal of the carrier. Initially, two methods were tested. (1) 30 G needles, filled with epoxy to prevent brain boring with the probe attached using PEG (**Figure 7A**), (2) half needles with a *U*-shaped cross section ("stylet"), made by grinding half of a 25 G needle using a Dremel sanding disk, with the probe placed in the groove and filled with PEG (**Figure 7B**).

The optimized insertion strategy used a carrier comprising a sharp steel electrode within a 25 G syringe needle, secured in place with two-part epoxy. The probe with incorporated ribbon cable was then mildly thermoformed with a hot air gun (~120°C) to straighten the ribbon cable, for easier attachment to the insertion device. The probe was attached with a thin PEG layer (**Figure 7C**), with a thicker layer used for attaching the connector. Using this method, it was possible to attach multiple electrodes to a single carrier, allowing up to four probes to be implanted during a single brain penetration (**Figure 7D**) with the use of a standard stereotax (Kopf, USA).

IMPEDANCE CHARACTERIZATION

Electrode impedances at 1 kHz in saline (IMP-1 meter, Bak Electronics, USA) were characterized for the probes (**Figure 8A**). A total of 426 recording sites were characterized, and impedance values all fell within the acceptable range for single-unit recordings <5 MΩ (Ludwig et al., 2011). Specifically, impedance values (±SEM) were 770 ± 15 kΩ.

The microfabrication process therefore produced many viable electrodes toward the end of the optimization period with many probes falling in the acceptable impedance range for single-unit recordings. The majority of probes (>83%) had impedances ≤1.2 MΩ, which is classed as good/ideal from data corresponding to the use of acute single shanked microwire probes (Microprobe Inc., USA) to isolate single-unit activity (Soteropoulos and Baker, 2009; Witham and Baker, 2012).

Electrode impedances were also fully characterized over a 180-day indwelling period for 15 electrode-recording sites (**Figure 8B**). There was no significant difference for explanted devices when comparing the impedance values at 1 kHz in saline (recording day 0 vs. 180, *t*-test: $t = 1.7$, $P > 0.05$). The mean impedance values for recording day 0 and 180 were 1100 ± 150 kΩ ($n = 15$ sites) and 850 ± 120 kΩ ($n = 12$ sites), respectively. This showed that the parylene-C-based devices were stable and survived damage, which could have been caused by the long indwelling period.

RECORDING DATA

This probe has registered high fidelity neural activity for over a 2-year period. Consistent waveforms were extracted with stable signal-to-noise ratio (SNR) and mean peak-to-peak amplitude over the recording period. The second probe generation could

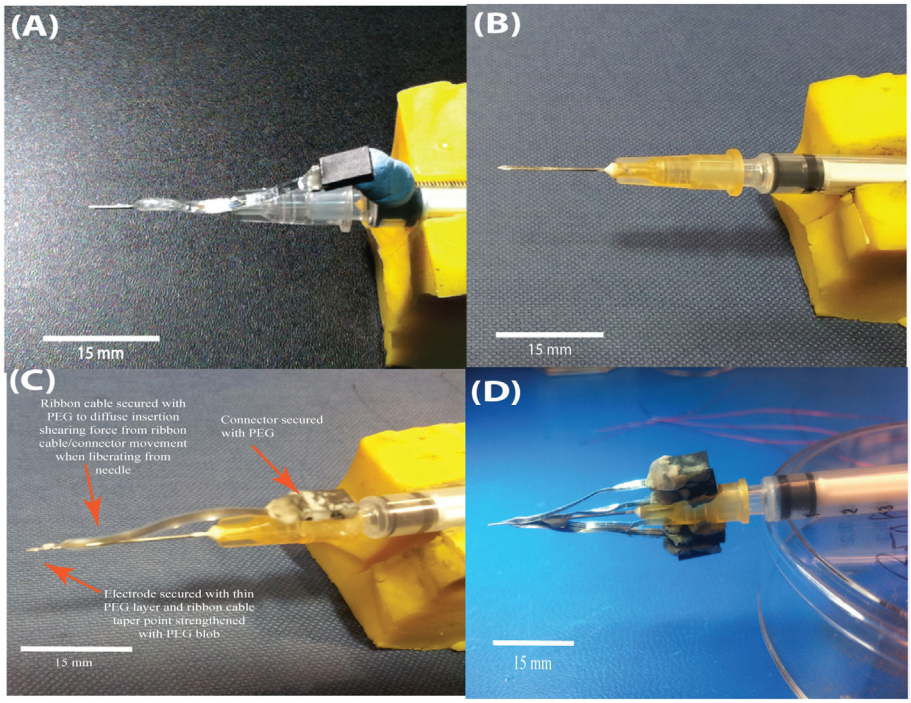

FIGURE 7 | Evolution of a relatively cheap insertion carrier to aid insertion of the flexible sinusoidal probe into the brain. Initial 30 G needles, epoxy filled were used **(A)**, but the probe "slid" upon insertion. Machined syringes with a groove were then considered **(B)**. The optimal device was a 25 G needle with a sharp steel electrode placed inside, with only the sharp steel electrode entering the brain **(C)**. The connector and probe were attached temporarily with PEG. Further, we optimized the insertion device to carry up to four sinusoidal probes **(D)**.

register neural activity for 140-day period with increasing SNR and peak-to-peak amplitude over the recording period ($n = 15$ recording sites, five probes) (Sohal et al., 2014). These promising initial recordings highlight the stability of the implanted probes and emphasize the reliable microfabrication process that has been developed, which promotes device survival for long indwelling periods.

As the probe can also be permanently attached to the carrier with two-part epoxy, a novel dual-purpose probe for both acute and chronic recording can be created.

As a demonstration of this, we show that we can acutely record from the mouse cortex with good SNR (**Figure 9**) following Suner's method (Suner et al., 2005; Ward et al., 2009). Experiments were approved by the local ethics committee at Newcastle University and appropriate UK Home Office licenses in accordance with the Animals (Scientific Procedures) Act 1986.

From example waveforms extracted ($n = 6$, **Figure 9B**), we showed good mean peak-to-peak amplitude (200 ± 50 uV), noise (33 ± 7 uV), and SNR (6.0 ± 0.5). For the signal, the peak-to-peak amplitude (A) of the mean waveform was calculated. For the noise, the mean waveform was subtracted from all waveforms, with the SD calculated from the resulting values. Noise was then calculated as 2× the average SD (ϵ). SNR was then calculated as A/ϵ. For 12 recording sites, there was no difference in pre- and post-implant impedance value post-device cleaning with ethanol and deionized water (t-test: $t = 1$, $P > 0.05$; **Figure 9C**).

The probes are parylene-C-based, so they are easier to clean than conventional silicon probes that have been used for repeated acute recordings due to minimized adhesion of tissue and blood following acute probe explant (Winslow et al., 2010).

DISCUSSION

The recording parameters and *in vivo* impedance measurements showed that the probe was reliable during the long indwelling periods, indicating a highly reliable microfabrication process. Current state-of-the-art probes have been reported to lose signal quality over a few weeks implantation period (Jackson and Fetz, 2007; Dickey et al., 2009), with device delamination post-explantation over these short periods (Barrese et al., 2013).

A change from SiO_2 to Al for the sacrificial layer allowed reliable release for the probe, as long as there was good adhesion between the Al and parylene-C. Al has a tendency to develop a thin native oxide over time, and this can interact with the silane-based (A-174) adhesion promoter used for parylene-C. Literature suggests that a greater oxide formation combined with silane will lead to enhanced adhesion between parylene-C and Al (Mitchell et al., 2006). Therefore, to enhance Al adhesion to parylene-C, a native oxide layer should be allowed to form on the Al through a simple delay in microfabrication processing, before parylene-C deposition. This will ensure there is reliable good adhesion. Although some other groups do not use a sacrificial layer with parylene-C or polyimide while demonstrating chronic usage up

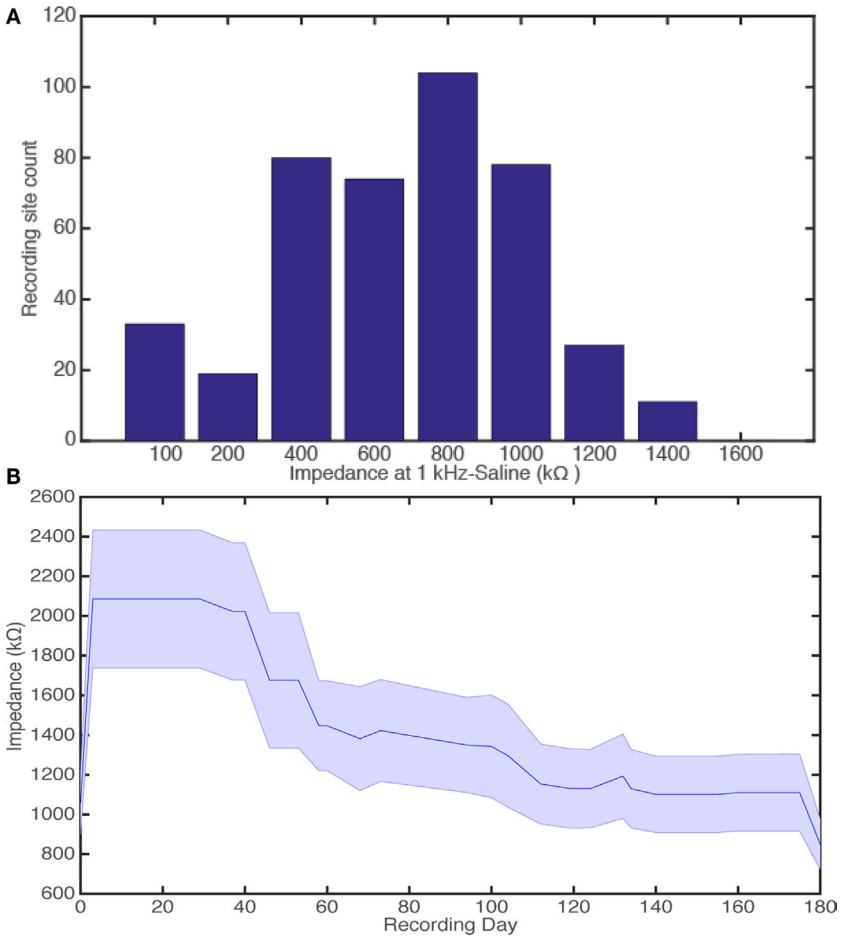

FIGURE 8 | Histogram for device impedance of 426 recording sites, binned every 200 kΩ. We show that all impedance measurements of recording sites at 1 kHz in saline are at suitable impedances for single-unit recording **(A)**. Electrode impedances over a 180-day indwelling period for 15 electrode-recording sites the second generation probe **(B)**. Day 0 and 180 equate to bench testing, measuring impedances at 1 kHz in saline for pre-implant and, where possible, explanted devices, respectively. The days in between are a measure of the electrode impedance at the electrode-tissue interface in the rabbit cortex.

to 28 days (Kim et al., 2013; Kuo et al., 2013), it was found here that device release was more reliable with it present.

Other groups have baked parylene-C with a nitrogen backflow to increase adhesion between the two layers (Kuo et al., 2013). But a slight over-etch of the metal roughens the first parylene-C layer surface leading to good device adhesion with no delamination to microfabricated, implanted, and explanted devices, as corroborated through impedance measurements and Raman spectroscopy. However, baking should be considered in future, especially with the incorporation of noble metals (e.g., platinum for chronic stimulation) to increase adhesion. Baking the parylene-C-based devices post-microfabrication between 200 and 300°C for 1–2 h may increase longevity of the Parylene-C. For saline-soaked samples at 37°C over a 300-day period, stable DC resistances of samples were observed at 300°C. Furthermore, comparing untreated, 200°C and 300°C samples, it was found that the baseline Yield strength of parylene-C can be enhanced with increasing temperature (77–107 MPa) (Von Metzen and Stieglitz, 2013).

A striking feature is that our devices remained stable for a 2-year indwelling period. Although there have been reports of parylene-C failure on intracortical probes, this is mainly due to deposition onto silicon. For the Utah array, thin (<4 μm) layers are used to insulate the array, and this will eventually break down due to adhesion of the parylene-C to the silicon (Barrese et al., 2013; Xie et al., 2014). Material stresses due to the *E* mismatch between silicon and parylene-C can also cause cracking (Kozai et al., 2014). No such problems were encountered with our probes when explanted, as similar impedance values were found pre- and postimplantation (**Figure 7B**). Probes were able to record for 2 years without degradation in the acquired neural signal, emphasizing material stability (Sohal et al., 2014). Literature suggests that parylene-C failure mechanisms include water and salts diffusion (Yasuda et al., 2001; Seymour et al., 2009), interfacial delamination (Barrese et al., 2013), and pinholes (Pierstorff et al., 2008). However, to mitigate this, the thick (although still flexible) parylene-C layers and minimized damage during processing (e.g., enhancing adhesion between layers) used in this study,

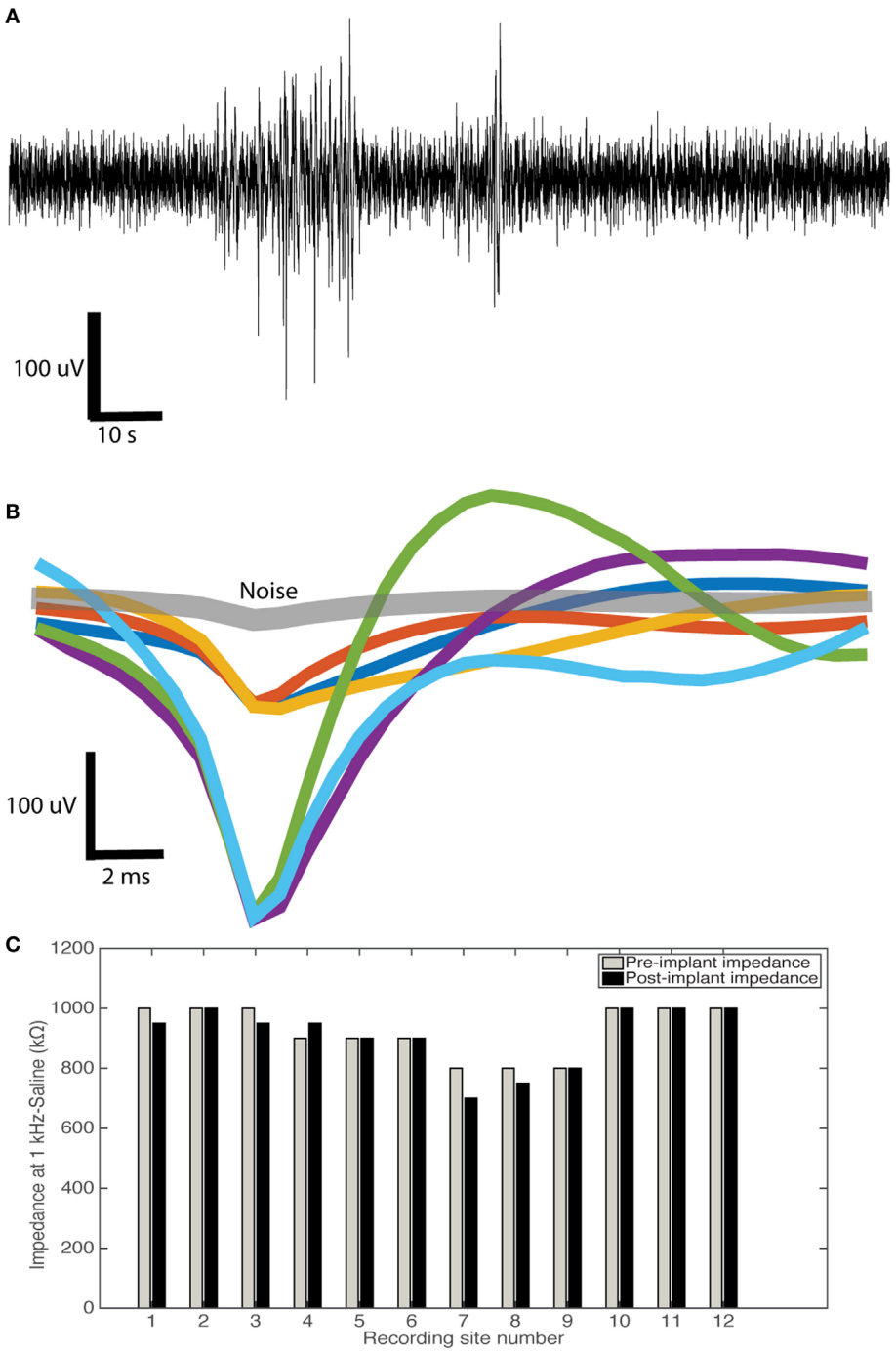

FIGURE 9 | **Sinusoidal probe acute neural recording example**. **(A)** Example 250 Hz high passed raw signal acquired showing good neural activity. **(B)** Overlain average waveforms of isolated units ($n = 6$) in comparison to noise waveforms (gray) isolated from a sinusoidal probe. We showed good: mean peak-to-peak amplitude (200 ± 49 uV), noise (33 ± 7 uV), and SNR (6.0 ± 0.5). **(C)** Impedance measurements pre- and post-implant for 12 recording sites (four probes) showing no change in impedance (t-test: $t = 1$, $P > 0.05$).

may have contributed to this improved chronic performance. Interestingly, a reduction in the microglia response was observed around the probes for a 12- and 24-month period (Sohal et al., 2014). Microglia are known to produce toxic chemicals, such as reactive oxygen species, that will degrade electrode material over time (Takmakov et al., 2015). A combination of overall design measures (**Figure 1**), material choice, and reduced gliosis may have contributed to the enhanced longevity of the probe.

Polyimide was found to contain many pinhole defects and therefore reaffirmed the choice for parylene-C use as an insulator.

Here, the acute recording qualities of the sinusoidal probe are demonstrated. The probe is permanently attached to the insulated sharp steel electrode and is further insulated from the effects of electromagnetic cross talk by using a two-part epoxy attachment technique. Good SNR and signal amplitude are observed, which are comparable, and in some cases, better than conventional silicon probes that are used in acute animal preparations (Blanche et al., 2005; Du et al., 2011; Berenyi et al., 2014). The reduced cost and ease of cleaning makes it an attractive alternative to silicon probes for both acute and chronic applications.

In addition to our stable devices, reduced gliosis responses were shown, compared with microwire electrodes (the gold standard in terms of gliosis at the time of the study) at 6-, 12-, and 24-month time points at the electrode tip, with an increase in neural integration around our probe (Sohal et al., 2014). This suggests that the design features incorporated in our probe have reduced the effects of micromotion-induced trauma.

Although these probes were restricted to 3 mm in size and three electrode-recording sites, this can be upscaled from a basic successful proof-of-concept design to allow for differing lengths and recording site arrangements. The design could potentially be adapted for multiple applications and differing species.

CONCLUSION

We have successfully microfabricated a reliable flexible probe for chronic neural recording, with one of the longest chronic indwelling periods (>2 years), without delamination. We have optimized etching of thick parylene-C layers and WTi metal. We have also developed a reliable device release strategy incorporating an aluminum release layer and TMAH, leading to a high number of functional devices. Further, we have developed a relatively simple and inexpensive device insertion technique that has been reliably used to insert the flexible devices into rabbit brains. This microfabrication process flow can also be applied to construct other flexible electrode types.

AUTHOR CONTRIBUTIONS

HS, AJ, and SB designed the novel electrode. HS performed the microfabrication, implant construction, electrophysiology recording, and subsequent analyses. KV aided in microfabrication techniques and design. HS, AJ, SB, and AO designed the experiments. All authors aided in the writing of this manuscript. AJ, SB, and AO equally contributed to this study.

FUNDING

This work was supported by the Wellcome Trust, EPSRC, and MRC.

REFERENCES

Baker, S., Burdess, J., Harris, A., Jackson, R., and Jackson, A. (2008). *Electrode-WO 2010035036 A3*. Available at: http://www.google.com/patents/WO2010035036A3?cl=fi

Barrese, J. C., Rao, N., Paroo, K., Triebwasser, C., Vargas-Irwin, C., Franquemont, L., et al. (2013). Failure mode analysis of silicon-based intracortical microelectrode arrays in non-human primates. *J. Neural Eng.* 10, 66014. doi:10.1088/1741-2560/10/6/066014

Berenyi, A., Somogyvári, Z., Nagy, A. J., Roux, L., Long, J. D., Fujisawa, S., et al. (2014). Large-scale, high-density (up to 512 channels) recording of local circuits in behaving animals. *J. Neurophysiol.* 111, 1132–1149. doi:10.1152/jn.00785.2013

Blanche, T. J., Spacek, M. A., Hetke, J. F., and Swindale, N. V. (2005). *Polytrodes: High-Density Silicon Electrode Arrays for Large-Scale Multiunit Recording*. Vancouver, BC: Department of Ophthalmology and Visual Sciences, University of British Columbia.

Canales, A., Jia, X., Froriep, U. P., Koppes, R. A., Tringides, C. M., Selvidge, J., et al. (2015). Multifunctional fibers for simultaneous optical, electrical and chemical interrogation of neural circuits in vivo. *Nat. Biotechnol.* 33, 277–284. doi:10.1038/nbt.3093

Chen, T., Xue, Z., Wang, C., Qu, Z., Wong, K. K., and Wong, S. T. C. (2010). "Motion artifact correction of multi-photon imaging of awake mice models using speed embedded HMM," in *Medical Image Computing and Computer-Assisted Intervention-MICCAI 2010* (Beijing: Springer), 473–480.

Collinger, J. L., Wodlinger, B., Downey, J. E., Wang, W., Tyler-Kabara, E. C., Weber, D. J., et al. (2013). High-performance neuroprosthetic control by an individual with tetraplegia. *Lancet* 381, 557–564. doi:10.1016/S0140-6736(12)61816-9

Dickey, A. S., Suminski, A., Amit, Y., and Hatsopoulos, N. G. (2009). Single-unit stability using chronically implanted multielectrode arrays. *J. Neurophysiol.* 102, 1331–1339. doi:10.1152/jn.90920.2008

Du, J., Blanche, T. J., Harrison, R. R., Lester, H. A., and Masmanidis, S. C. (2011). Multiplexed, high density electrophysiology with nanofabricated neural probes. *PLoS ONE* 6:e26204. doi:10.1371/journal.pone.0026204

Gilletti, A., and Muthuswamy, J. (2006). Brain micromotion around implants in the rodent somatosensory cortex. *J. Neural Eng.* 3, 189–195. doi:10.1088/1741-2560/3/3/001

Guitchounts, G., Markowitz, J. E., Liberti, W. A., and Gardner, T. J. (2013). A carbon-fiber electrode array for long-term neural recording. *J. Neural Eng.* 10, 46016. doi:10.1088/1741-2560/10/4/046016

Harris, J. P., Capadona, J. R., Miller, R. H., Healy, B. C., Shanmuganathan, K., Rowan, S. J., et al. (2011a). Mechanically adaptive intracortical implants improve the proximity of neuronal cell bodies. *J. Neural Eng.* 8, 66011. doi:10.1088/1741-2560/8/6/066011

Harris, J. P., Hess, A. E., Rowan, S. J., Weder, C., Zorman, C. A., Tyler, D. J., et al. (2011b). In vivo deployment of mechanically adaptive nanocomposites for intracortical microelectrodes. *J. Neural Eng.* 8, 46010. doi:10.1088/1741-2560/8/4/046010

Hess, A. E., Capadona, J. R., Shanmuganathan, K., Hsu, L., Rowan, S. J., Weder, C., et al. (2011). Development of a stimuli-responsive polymer nanocomposite toward biologically optimized, MEMS-based neural probes. *J. Micromech. Microeng.* 21, 54009. doi:10.1088/0960-1317/21/5/054009

Hochberg, L. R., Bacher, D., Jarosiewicz, B., Masse, N. Y., Simeral, J. D., Vogel, J., et al. (2012). Reach and grasp by people with tetraplegia using a neurally controlled robotic arm. *Nature* 485, 372–375. doi:10.1038/nature11076

Hochberg, L. R., Serruya, M. D., Friehs, G. M., Mukand, J. A., Saleh, M., Caplan, A. H., et al. (2006). Neuronal ensemble control of prosthetic devices by a human with tetraplegia. *Nature* 442, 164–171. doi:10.1038/nature04970

Hubel, D. H. (1959). Single unit activity in striate cortex of unrestrained cats. *J. Physiol.* 147, 226–238. doi:10.1113/jphysiol.1959.sp006238

Jackson, A., and Fetz, E. E. (2007). Compact movable microwire array for long-term chronic unit recording in cerebral cortex of primates. *J. Neurophysiol.* 98, 3109–3118. doi:10.1152/jn.00569.2007

Kim, B. J., Kuo, J. T. W., Hara, S. A., Lee, C. D., Yu, L., Gutierrez, C. A., et al. (2013). 3D parylene sheath neural probe for chronic recordings. *J. Neural Eng.* 10, 45002. doi:10.1088/1741-2560/10/4/045002

Köhler, P., Wolff, A., Ejserholm, F., Wallman, L., Schouenborg, J., and Linsmeier, C. E. (2015). Influence of probe flexibility and gelatin embedding on neuronal density and glial responses to brain implants. *PLoS ONE* 10:e0119340. doi:10.1371/journal.pone.0119340

Kozai, T. D. Y., Catt, K., Li, X., Gugel, Z. V., Olafsson, V. T., Vazquez, A. L., et al. (2014). Biomaterials mechanical failure modes of chronically implanted planar silicon-based neural probes for laminar recording. *Biomaterials* 37, 1–15. doi:10.1016/j.biomaterials.2014.10.040

Kuo, J. T. W., Kim, B. J., Hara, S. A., Lee, C. D., Gutierrez, C. A., Hoang, T. Q., et al. (2013). Novel flexible parylene neural probe with 3D sheath structure for enhancing tissue integration. *Lab. Chip* 13, 554–561. doi:10.1039/c2lc40935f

Loeb, G. E., Bak, M. J., Salcman, M., and Schmidt, E. M. (1977). Parylene as a chronically stable, reproducible microelectrode insulator. *IEEE Trans. Biomed. Eng.* 24, 121–128. doi:10.1109/TBME.1977.326115

Lu, C., Froriep, U. P., Koppes, R. A., Canales, A., Caggiano, V., Selvidge, J., et al. (2014). Polymer fiber probes enable optical control of spinal cord and muscle function in vivo. *Adv. Funct. Mater.* 24, 6594–6600. doi:10.1002/adfm.201401266

Ludwig, K. A., Langhals, N. B., Joseph, M. D., Richardson-Burns, S. M., Hendricks, J. L., and Kipke, D. R. (2011). Poly(3,4-ethylenedioxythiophene) (PEDOT) polymer coatings facilitate smaller neural recording electrodes. *J. Neural Eng.* 8, 14001. doi:10.1088/1741-2560/8/1/014001

Mitchell, C. J., Yang, G.-R., and Senkevich, J. J. (2006). Adhesion aspects of poly(p-xylylene) to SiO2 surfaces using γ-methacryloxypropyltrimethoxysilane as an adhesion promoter. *J. Adhes. Sci. Technol.* 20, 1637–1647. doi:10.1163/156856106778884217

Patel, P. R., Na, K., Zhang, H., Kozai, T. D. Y., Kotov, N. A., Yoon, E., et al. (2015). Insertion of linear 8.4 μm diameter 16 channel carbon fiber electrode arrays for single unit recordings. *J. Neural Eng.* 12, 046009. doi:10.1088/1741-2560/12/4/046009

Pierstorff, E., Lam, R., and Ho, D. (2008). Nanoscale architectural tuning of parylene patch devices to control therapeutic release rates. *Nanotechnology* 19, 445104. doi:10.1088/0957-4484/19/44/445104

Polikov, V. S., Tresco, P. A., and Reichert, W. M. (2005). Response of brain tissue to chronically implanted neural electrodes. *J. Neurosci. Methods* 148, 1–18. doi:10.1016/j.jneumeth.2005.08.015

Poncelet, B. P., Wedeen, V. J., Weisskoff, R. M., and Cohen, M. S. (1992). Brain parenchyma motion: measurement with cine echo-planar MR imaging. *Radiology* 185, 645–651. doi:10.1148/radiology.185.3.1438740

Ceyssens, F., and Puers, R. (2015). Insulation lifetime improvement of polyimide thin film neural implants. *J. Neural Eng.* 12, 54001. doi:10.1088/1741-2560/12/5/054001

Rubehn, B., Bosman, C., Oostenveld, R., Fries, P., and Stieglitz, T. (2009). A MEMS-based flexible multichannel ECoG-electrode array. *J. Neural Eng.* 6, 36003. doi:10.1088/1741-2560/6/3/036003

Rubehn, B., and Stieglitz, T. (2007). Measurement of defects in spin coated polyimide films. *Conf. Proc. IEEE Eng. Med. Biol. Soc.* 2007, 183–185. doi:10.1109/IEMBS.2007.4352253

Seymour, J. P., Elkasabi, Y. M., Chen, H.-Y. Y., Lahann, J., and Kipke, D. R. (2009). The insulation performance of reactive parylene films in implantable electronic devices. *Biomaterials* 30, 6158–6167. doi:10.1016/j.biomaterials.2009.07.061

Seymour, J. P., and Kipke, D. R. (2007). Neural probe design for reduced tissue encapsulation in CNS. *Biomaterials* 28, 3594–3607. doi:10.1016/j.biomaterials.2007.03.024

Seymour, J. P., Langhals, N. B., Anderson, D. J., and Kipke, D. R. (2011). Novel multi-sided, microelectrode arrays for implantable neural applications. *Biomed. Microdevices* 13, 441–451. doi:10.1007/s10544-011-9512-z

Sohal, H. S., Jackson, A., Jackson, R., Clowry, G. J., Vassilevski, K., O'Neill, A., et al. (2014). The sinusoidal probe: a new approach to improve electrode longevity. *Front. Neuroeng.* 7:10. doi:10.3389/fneng.2014.00010

Soteropoulos, D. S., and Baker, S. N. (2009). Quantifying neural coding of event timing. *J. Neurophysiol.* 101, 402–417. doi:10.1152/jn.90767.2008

Subbaroyan, J., Martin, D. C., and Kipke, D. R. (2005). A finite-element model of the mechanical effects of implantable microelectrodes in the cerebral cortex. *J. Neural Eng.* 2, 103–113. doi:10.1088/1741-2560/2/4/006

Suner, S., Fellows, M. R., Vargas-Irwin, C., Nakata, G. K., and Donoghue, J. P. (2005). Reliability of signals from a chronically implanted, silicon-based electrode array in non-human primate primary motor cortex. *IEEE Trans. Neural Syst. Rehabil. Eng* 13, 524–541.

Takmakov, P., Ruda, K., Phillips, K. S., Isayeva, I. S., Krauthamer, V., and Welle, C. G. (2015). Rapid evaluation of the durability of cortical neural implants using accelerated aging with reactive oxygen species. *J. Neural Eng.* 12, 26003. doi:10.1088/1741-2560/12/2/026003

Tooker, A., Tolosa, V., Shah, K. G., Sheth, H., Felix, S., Delima, T., et al. (2012). Polymer neural interface with dual-sided electrodes for neural stimulation and recording. *Conf. Proc. IEEE Eng. Med. Biol. Soc.* 2012, 5999–6002. doi:10.1109/EMBC.2012.6347361

Von Metzen, R. P., and Stieglitz, T. (2013). The effects of annealing on mechanical, chemical, and physical properties and structural stability of parylene C. *Biomed. Microdevices* 15, 727–735. doi:10.1007/s10544-013-9758-8

Ward, M. P., Rajdev, P., Ellison, C., and Irazoqui, P. P. (2009). Toward a comparison of microelectrodes for acute and chronic recordings. *Brain Res.* 1282, 183–200. doi:10.1016/j.brainres.2009.05.052

Ware, T., Simon, D., Arreaga-Salas, D. E., Reeder, J., Rennaker, R., Keefer, E. W., et al. (2012). Fabrication of responsive, softening neural interfaces. *Adv. Funct. Mater.* 22, 3470–3479. doi:10.1002/adfm.201200200

Williams, K. R., Gupta, K., and Wasilik, M. (2003). Etch rates for micromachining processing-part II. *J. Microelectromech. Syst.* 12, 761–778. doi:10.1109/JMEMS.2003.820936

Winslow, B. D., Christensen, M. B., Yang, W.-K., Solzbacher, F., and Tresco, P. A. (2010). A comparison of the tissue response to chronically implanted parylene-C-coated and uncoated planar silicon microelectrode arrays in rat cortex. *Biomaterials* 31, 9163–9172. doi:10.1016/j.biomaterials.2010.05.050

Witham, C. L., and Baker, S. N. (2012). Coding of digit displacement by cell spiking and network oscillations in the monkey sensorimotor cortex. *J. Neurophysiol.* 108, 3342–3352. doi:10.1152/jn.00462.2012

Xie, X., Rieth, L., Williams, L., Negi, S., Bhandari, R., Caldwell, R., et al. (2014). Long-term reliability of Al2O3 and parylene C bilayer encapsulated Utah electrode array based neural interfaces for chronic implantation. *J. Neural Eng.* 11, 26016. doi:10.1088/1741-2560/11/2/026016

Yasuda, H., Yu, Q. S., and Chen, M. (2001). Interfacial factors in corrosion protection: an EIS study of model systems. *Prog. Org. Coat.* 41, 273–279. doi:10.1016/S0300-9440(01)00142-4

Yoshida Kozai, T. D., Langhals, N. B., Patel, P. R., Deng, X., Zhang, H., Smith, K. L., et al. (2012). Ultrasmall implantable composite microelectrodes with bioactive surfaces for chronic neural interfaces. *Nat. Mater.* 11, 1065–1073. doi:10.1038/nmat3468

Conflict of Interest Statement: The authors declare that the research was conducted in the absence of any commercial or financial relationships that could be construed as a potential conflict of interest.